https://dx.doi.org/10.21577/0103-5053.20220140

J. Braz. Chem. Soc., Vol. 34, No. 5, 694-704, 2023

Article

Effect of *Camellia sinensis* Origin and Heat Treatment in the Iron Oxides Nanomaterials Composition and Fenton Degradation of Methyl Orange

Raissa T. Franco, [a] ***Ana Luisa Silva,*** [a] ***Yordy E. Licea,*** [#,b] ***Mariella Alzamora,*** [c] ***Dalber R. Sánchez*** [d] ***and Nakédia M. F. Carvalho*** [*,a]

[a]*Instituto de Química, Universidade do Estado do Rio de Janeiro, Rua São Francisco Xavier, 524, Edifício Haroldo Lisboa da Cunha, room 312a, Maracanã, 20550-013 Rio de Janeiro-RJ, Brazil*

[b]*Centro Brasileiro de Pesquisas Físicas (CBPF), COMAN/CBPF, Rua Dr. Xavier Sigaud, 150, Urca, 22290-180 Rio de Janeiro-RJ, Brazil*

[c]*Universidade Federal do Rio de Janeiro, Campus Duque de Caxias, 25240-005 Duque de Caxias-RJ, Brazil*

[d]*Instituto de Física, Universidade Federal Fluminense, Av. Gal. Milton Tavares de Souza, Gragoatá, 24210-346 Niterói-RJ, Brasil*

Sustainable and environmentally friendly methods for nanomaterials synthesis have been emerging recently. The use of extracts of polyphenol-rich plants with high reducing and chelating power is advantageous because the polyphenol can protect the nanomaterial from agglomeration and deactivation. Green nanomaterials have been applied in several areas, including remediation of toxic organic pollutants from contaminated effluents. Herein, we describe the preparation of green iron oxide nanoparticles (IONPs) with extracts of the plant *Camellia sinensis* as black tea for dye removal application. The as-prepared IONPs were composed of amorphous FeOOH and $Fe^{II/III}$-polyphenol complexes. To obtain crystalline and pure iron-based nanomaterials, the amorphous precursor was annealed at 900 ºC. Samples of black tea from different regions were used to verify the reproducibility of the iron phases formed. The same iron phases were obtained for all black tea samples, α-Fe_2O_3 (hematite), $FePO_4$, and Fe_3PO_7, but in different proportions. The materials were applied as heterogeneous-Fenton catalysts for the removal of the dye methyl orange. The amorphous as-prepared IONPs were more active than the respective annealed IONPs due to the proton release from the polyphenol into the reaction medium, setting the pH to around 3, which is the optimum pH for the Fenton system.

Keywords: iron oxide, iron phosphate, polyphenols, black tea, methyl orange, Fenton

Introduction

Environmentally friendly synthesis of nanomaterials has been emerging in recent years. The use of extracts of polyphenol-rich plants and biomass residues has gained much attention in the preparation of metal and metal oxides nanoparticles.[1-3] Polyphenols is a class of compounds that includes caffeine, flavanol, theaflavins, thearubigins, catechins and polymeric pigments, among others.[4,5] Polyphenols can chelate to the metal ion through the hydroxyl groups and at the same time can reduce, functionalize, and stabilize the nanoparticles formed, which prevents nanoparticles agglomeration, deactivation, and produces more stable nanomaterials.[6]

Green iron oxide nanoparticles (IONPs) prepared with plant extracts have been extensively investigated in recent years.[1-3] Different plants as black tea, Yerba Mate, grape seed, green tea, oolong tea, eucalyptus leaf, have produced different iron nanomaterials because of the different polyphenol composition and synthesis condition, which consequently affects the IONPs properties.[6-15] As reported in the literature,[6-10] most of the green IONPs are amorphous materials due to the high content of polyphenols, which precludes formation of defined crystalline nanomaterials as well as formation of iron oxides of scientific and technological interest.

*e-mail: nakedia@uerj.br
Editor handled this article: Izaura C. N. Diógenes (Associate)
#Present address: GSK Biopharma Production Dept. 9910 Belward Campus Dr, Rockville, MD 20850 USA

Thermal treatment has been described for green IONPs to favor the formation of crystalline and well-defined iron oxides. For instance, IONPs prepared from Fe^{III} and *Aegle marmelos* or avocado fruit rind extracts were thermally treated at 400 °C and the formation of α-Fe_2O_3 were observed.[16,17] The reaction of Fe^{II} with *Sageretia thea* extract led to the formation of highly crystalline and pure γ-Fe_2O_3 phase after annealing at 500 °C.[18] Recently, we have reported the effect of thermal treatment in the range of 400 to 900 °C on the IONPs properties prepared from black tea extract.[19] A thorough characterization of the samples allowed the assignment of the as-prepared amorphous IONPs as FeOOH and Fe^{II}/Fe^{III}-polyphenols complexes. After the continuous removal of polyphenols while rising the temperature, the concomitant formation of crystalline iron phases took place. The Fe^{III} oxides α-Fe_2O_3 and β-Fe_2O_3 were gradually formed along with the formation of $FePO_4$ and Fe_3PO_7. The phosphorous origin was attributed to the black tea leaves.[19] However, a question of whether these iron phases would always be formed from different samples of black tea still needed to be addressed.

The main application reported for green IONPs is in environmental remediation, such as organic contaminant removal from industrial effluents. Improper disposal of toxic and recalcitrant pollutants is a major problem since it brings serious risks to the health of living beings and causes environmental deterioration.[20,21] The removal of dyes commonly found in industrial effluents by IONPs has been extensively studied,[22-28] among them the heterogeneous Fenton system plays a central role to mineralize the contaminant.[2,6-8,10,11] IONPs prepared by a green route with extracts of black tea,[7] Yerba Mate,[6,8] and green tea,[11] were applied in the degradation of the dye methyl orange. Furthermore, the green IONPs exhibit special advantages for the Fenton process, as restoration of Fe^{II} from the reduction of Fe^{III} by the polyphenol; improvement of Fe^{II} stability and prevention of iron sludge formation by the polyphenols 'protection; and enhancement of OH· radicals formation by the hydrogen releasing from the polyphenols that can adjust the reaction pH to around 3, which is the ideal pH for Fenton process operation.[1]

In this work we have prepared green IONPs with three black tea extracts from different regions and have annealed the samples at 900 °C to provide crystalline iron compounds of interest for environmental remediation. The materials were characterized thoroughly and the effect of the tea origin in the reproducibility of the IONPs properties and phase composition was evaluated. The green as-prepared and annealed iron nanomaterials were applied in the heterogeneous Fenton degradation of the azo dye methyl orange. The degradation kinetics was also studied.

Experimental

Materials

All chemicals are of reagent grade and were used as received, unless otherwise specified. Black tea samples were purchased from Brazil, United States, and Nepal brands, in local markets in the respective country, and were named as BT1, BT2 and BT3, respectively. The black tea samples were composed of dried *Camellia sinensis* L. Kuntze leaves and stalks. Iron(III) chloride hexahydrate, Folin-Ciocalteu phenol reagent and hydrogen peroxide (30% water) were purchased from Sigma-Aldrich (St. Louis, MO, United States). Hydrogen peroxide was titrated by the iodometric method before use (9.23 mol L^{-1}). Methyl orange (MO) (Casa da Química, Diadema, SP, Brazil) was recrystallized before handling.

Synthesis of the iron oxide nanomaterials

The black tea extracts were prepared by heating 28.8 g of the plant and 480.0 mL of water (60.0 g L^{-1}) at 80 °C, under stirring for 60 min. The suspension was filtered under reduced pressure and the extract was used immediately.

The iron nanomaterials were prepared by the addition of 480.0 mL of the black tea extract to 240.0 mL of 0.096 mol L^{-1} $FeCl_3 \cdot 6H_2O$ (6.22 g) aqueous solution, under stirring, at room temperature, during 40 min. After, the reaction was stirred for 1 h, and the black solid were filtered off, washed with water and ethanol, and dried at 75 °C for 3 days. The materials were named ^{BTn}Fe according to the black tea used, which was further calcined at 900 °C for 4 h under atmospheric air, producing the samples named $^{BTn}Fe_{900}$. The procedure was repeated for different black tea brands: Brazil (^{BT1}Fe), USA (^{BT2}Fe) and Nepal (^{BT3}Fe).

Methyl orange degradation tests

The methyl orange degradation tests were carried out in water, at room temperature, under magnetic stirring. In a vial, 10.0 mg of the iron nanomaterial, 2.0 mL of 4.7×10^{-4} mol L^{-1} dye solution resulting in a final concentration of $C_f = 4.7 \times 10^{-5}$ mol L^{-1}, 1.5 mL of 9.23 mol L^{-1} H_2O_2 resulting in a final concentration of $C_f = 0.69$ mol L^{-1}, and water to complete 20.0 mL of total volume were mixed. After a given time, aliquots of 1.0 mL were withdrawal, filtered through a 0.22 μm membrane filter, and the solution analyzed spectrophotometrically using a diode-array UV-VIS Agilent 8453 spectrophotometer (Santa Clara, CA, United States). The decolorization percentage was calculated using equation 1:

$$\text{Decolorization}\,(\%) = \frac{\text{Abs}_0 - \text{Abs}_t}{\text{Abs}_0} \times 100 \quad (1)$$

where Abs_0 is the absorbance of MO at time = 0, and Abs_t is the absorbance of MO at given time (min).

Characterization methods

X-ray fluorescence spectrometry (XRF) was used to determine the elemental composition of the black tea leaves, in a Bruker S8 Tiger (Billerica, MA, United States) instrument under He. The Folin-Ciocalteu method was used to determine the total polyphenol concentration (TPC) of the black tea extracts, and the results were expressed in milligram of gallic acid equivalents *per* gram of BT leaves (mg GA g^{-1}) (Table S1, Supplementary Information (SI) section).

The iron nanomaterials were characterized by X-ray diffraction (XRD) using a Rigaku Miniflex II X-Ray diffractometer (Rigaku®, Japan), monochromatic Cu Kα radiation (λ = 1.540 Å) in the 2θ angle range between 5 and 80°, at a step width of 0.05°, counting 1 min between each step. Fourier transform infrared spectroscopy (FTIR) spectra were acquired using a PerkinElmer Frontier Single & Dual Ranger (Waltham, MA, United States) spectrophotometer, in KBr pellets. ^{57}Fe Mössbauer spectroscopy (WissEl, Starnberg, Germany) were performed at room temperature, in transmission geometry with the samples and the ^{57}Co:Rh source moving sinusoidally. The hyperfine parameter isomer shift (δ) values were expressed in relation to α-iron foil. Scanning electron microscopy (SEM) images were obtained in a Jeol 7100FT (Japan) (LABNANO/CBBP) microscope equipped with an X-ray energy-dispersive spectrometer (EDS) 80 mm^2 single-shot detector (SDD), Oxford Instruments (Abingdon, United Kingdom), with the samples deposited over conducting FTO (fluorinated tin oxide) glass plates by drop casting a 10 mg mL^{-1} suspension in isopropyl alcohol over the FTO plate. Thermogravimetric analyses and differential thermal analysis (TGA/DTA) were acquired in a Netzsch (Selb, Germany) thermogravimetric system TG 209F1 Iris. 10.0 mg of the sample was placed in an alumina crucible and was heated from 35 to 900 °C, at 10 °C min^{-1}, under synthetic air (20 mL min^{-1}).

The methyl orange degradation was followed by electronic spectroscopy in ultraviolet-visible region (UV-Vis) region, in a diode-array Agilent 8453 spectrophotometer (Santa Clara, CA, United States) in water. Total organic carbon (TOC) analyses of the supernatant after reaction were conducted in a Shimadzu equipment, model TOC-L. Iron leaching of the iron nanomaterial caused by hydrogen peroxide in water at the same concentration of the Fenton tests, was evaluated by flame atomic absorption spectrometry (F AAS) in a iCE 3000 Series model, Thermo Analytica (Waltham, MA, United States) spectrometer.

Results and Discussion

Iron nanomaterials characterization

The green IONPs were prepared from $FeCl_3$ and the extract of the polyphenolic-rich plant *Camellia sinensis* in the form of black tea. We also attempted to investigate the effect of the thermal treatment on the formation of well-defined iron oxides nanomaterials. The reproducibility of the materials before and after annealing in respect to the black tea origin was investigated for three samples from different countries. TPC for the extracts of BT1, BT2 and BT3 was 46.0, 53.6, and 53.1 mg GA g^{-1}, respectively (Table S1), which is in the range for other plants used in IONPs synthesis.[29] Elemental composition determined by XRF showed C and H as the major elements with CH_2 around 98 wt.%, followed by K around 1 wt.%, and Ca, Mg, P and S in the order of 0.1 wt.%.

The powder XRD patterns of the as-prepared ^{BTn}Fe materials showed a large peak around 23° (Figure 1a), typical of amorphous IONPs coated with the polyphenols.[6-10] SEM images (Figure S1, SI section) showed particles of undefined and irregular shape, with a wide size range due to agglomeration. The corresponding EDS spectra of the sample ^{BT1}Fe in Figure 1b showed carbon and oxygen as the main elements around 60 and 35 at%, respectively. Comparatively, low amount of iron and phosphorous was detected, around 0.2 and 2.0 at%, respectively. Similar elemental composition and distribution was observed for ^{BT2}Fe and ^{BT3}Fe (Figures S2-S4, SI section), as summarized in Table 1. The EDS mapping images showed that the elements are homogenously distributed in all regions of the sample.

Thermogravimetric curves of ^{BTn}Fe were acquired under synthetic air and are characterized by three main regions of weight loss (Figure 2). Region I from 30 to 150 °C represents the humidity release around 13 wt.%. The regions II (150-500 °C) and III (500-900 °C) are assigned for degradation of organic compounds of different molecular weight from the polyphenols (Table S2, SI section), accounting for around 78 wt.% of the sample and confirming the high content of organic compounds (Table 1). The tea extracts with higher TPC also provided the higher organic contents (BT2 and BT3). These data are in accordance with the EDS analysis. DTA curves show that the main weight loss takes place around 400-450 °C. Furthermore, around 90 wt.% of the samples is decomposed

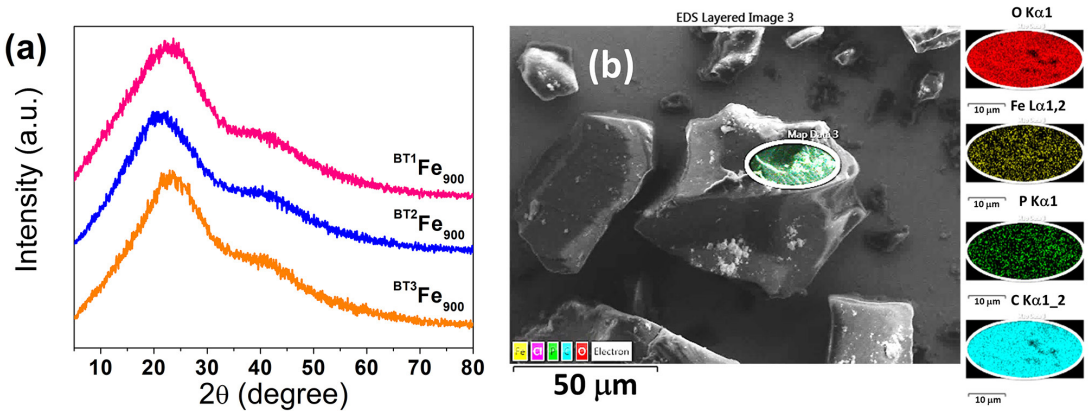

Figure 1. (a) XRD patterns of the as-prepared ^{BTn}Fe samples. (b) EDS mapping images of ^{BT1}Fe.

Table 1. Average atomic percentage[a] of all catalysts and organic content[b] of the as-prepared catalysts

Catalyst	C / at%	O / at%	Fe / at%	P / at%	Organic content / wt.%
^{BT1}Fe	62.5	37.2	0.1	0.2	77.0
^{BT1}Fe$_{900}$	8.3	56.9	26.9	8.3	–
^{BT2}Fe	46.8	44.9	0.2	0.05	78.3
^{BT2}Fe$_{900}$	4.4	27.6	57.9	10.2	–
^{BT3}Fe	74.3	23.2	0.2	2.2	80.3
^{BT3}Fe$_{900}$	7.0	49.1	36.5	6.6	–

[a]Measured from EDS spectra (Figures S2-S8, SI section); [b]estimated from thermogravimetric data (Table S2, SI section).

up to 900 °C, remaining only the IONPs, which accounted for 5.8-7.0 wt.% of iron (Table S2, SI section).

The as-prepared ^{BTn}Fe were annealed at 900 ºC, resulting in the ^{BTn}Fe$_{900}$ samples. The XRD patterns of ^{BTn}Fe$_{900}$ (Figure 3d) show peaks corresponding to α-Fe_2O_3 (hematite, JCPDS 33-0664), $FePO_4$ (rodolicoite, JCPDS 29-715), and Fe_3PO_7 (grattarolaite, JCPDS 37-61). However, the relative peak intensity of each phase varied according to the black tea used, the major phase in ^{BT1}Fe$_{900}$ corresponded to Fe_3PO_7, in ^{BT2}Fe$_{900}$ corresponded to α-Fe_2O_3, and ^{BT3}Fe$_{900}$ sample contained the largest amount of $FePO_4$. This assignment was corroborated by the refinement of ^{BT3}Fe$_{900}$ diffractogram by the Rietveld method (Figure S9, SI section). Moreover, these results agree with the Mössbauer data discussed below. XRD results of IONPs synthesized using *Aegle marmelos* and avocado fruit rind extracts, also showed formation of the iron oxide α-Fe_2O_3 when calcinated at 400 °C.[16,17] Similarly, the diffractogram of IONPs from *Sageretia thea* extract showed the formation of pure and crystalline γ-Fe_2O_3 after annealing at 500 °C.[18]

The presence of phosphates in the samples can be attributed to the phosphorous element present in the black tea leaves, which upon thermal treatment formed the Fe^{III} phosphates. From XRF analysis (Table S1), phosphorous

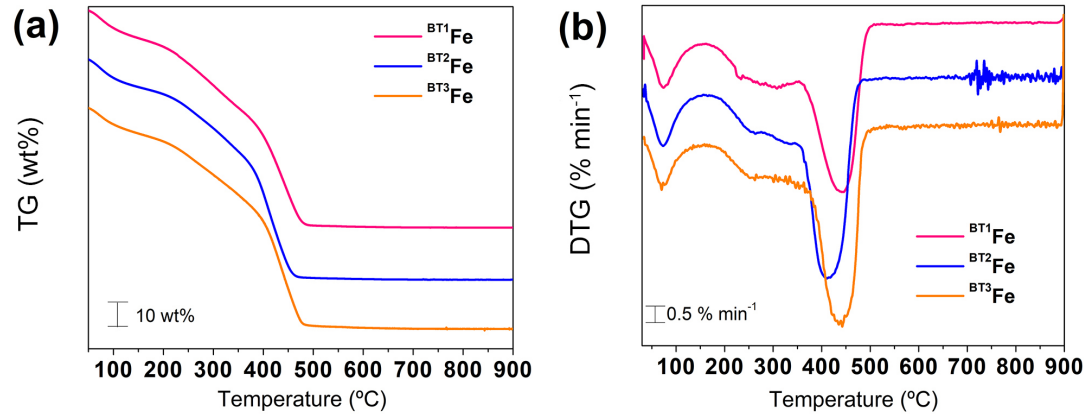

Figure 2. TG (a) and DTG (b) curves of the as-prepared ^{BTn}Fe samples.

accounted for 0.09-0.11 wt.% of the tea leaves, that is converted to the $FePO_4$ and Fe_3PO_7 phases. Considering the amount of Fe^{III} salt and black tea extract used in the synthesis, and that the BT1 dry leaves have 0.10 wt.% of P in the composition, it would form 0.140 g of $FePO_4$ or 0.289 g of Fe_3PO_7. The amount of $^{BT1}Fe_{900}$ formed after annealing at 900 °C was 0.250 g, close to the value of $FePO_4$ and Fe_3PO_7 estimated from the reagents used in the synthesis if all Fe^{III} produced these two phosphates. Fe^{III} phosphates of similar crystalline structures and Mössbauer parameters are commonly found naturally.[30] Iron biochar prepared from pyrolysis of dried distillers' grain at 900 °C under N_2 atmosphere also presented phosphites and the phosphorous origin was attributed to the biomass.[31]

Crystallite size of the iron nanomaterials was calculated by the Scherrer equation.[32] Crystallites smaller than 36 nm were observed for all iron phases present at the three $^{BTn}Fe_{900}$ samples. Comparing the different black tea extracts, it is possible to observe that the nanomaterials presented similar crystallite sizes after the thermal treatment (Table 2).

Figures 3a-3c show the SEM images of $^{BTn}Fe_{900}$, where it is possible to observe that the particles became more defined after the removal of the polyphenols at 900 °C. $^{BT2}Fe_{900}$ and $^{BT3}Fe_{900}$ adopted a similar spherical morphology, although $^{BT1}Fe_{900}$ still presented more agglomerated, undefined morphology. Particles of 512 nm of diameter could be observed for $^{BT2}Fe_{900}$, but most of them are outside the nanometer range, probably due to sintering at high temperature. EDS analyses (Table 1) confirmed the drastic removal of polyphenol with residual C around 7 at%, and a considerable increase in the amount of Fe to around 40 at%, P to around 9 at% and O to around 40 at%. The values are typical of the α-Fe_2O_3, $FePO_4$ and Fe_3PO_7 phases detected by XRD. From the EDS mapping of $^{BT1}Fe_{900}$ (Figure 3e) it is shown that the elements are homogeneously distributed in all regions of the sample. Similar elemental composition and distribution was observed for $^{BT2}Fe_{900}$ and $^{BT3}Fe_{900}$ (Figures S6-S8, SI section).

Table 2. Crystallite size of the iron nanomaterials of the samples $^{BTn}Fe_{900}$

Catalyst	Crystallite size / nm		
	Fe_3PO_7[a]	$FePO_4$[b]	α-Fe_2O_3[c]
$^{BT1}Fe_{900}$	25.9	28.2	35.5
$^{BT2}Fe_{900}$	26.2	27.2	33.3
$^{BT3}Fe_{900}$	29.5	29.9	31.5

[a]2θ = 28.8°; [b]2θ = 25.8°; [c]2θ = 35.5°.

^{57}Fe Mössbauer spectra of the as-prepared samples were collected at room temperature (Figure 4) and were properly fitted with three paramagnetic doublets and the corresponding hyperfine parameters of all the subspectra are shown in Table 3. Two of these subspectra, with the hyperfine parameters isomer shift δ ca. 0.44 mm s^{-1} and quadrupole splitting ΔE_Q ca. 0.81 mm s^{-1}, corresponds to Fe^{III} (Table 3) in akageneite-FeOOH, or ferrihydrite-$FeO(OH)\cdot nH_2O$.[6] Also, these two doublets can be attributed

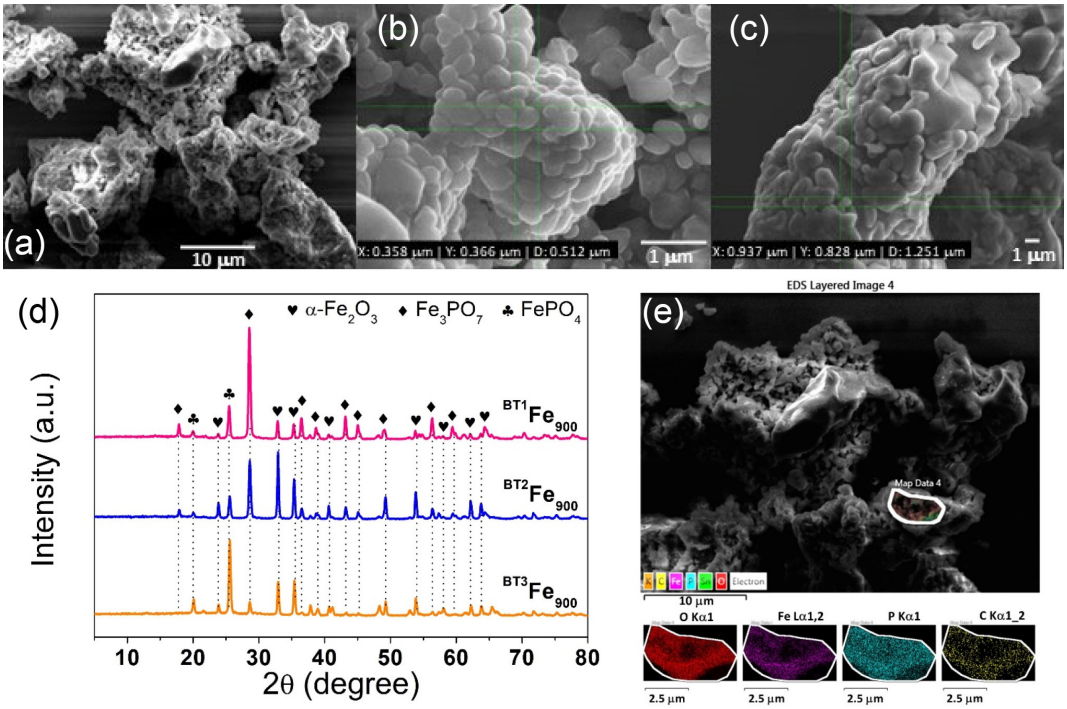

Figure 3. SEM images of (a) $^{BT1}Fe_{900}$, (b) $^{BT2}Fe_{900}$ and (c) $^{BT3}Fe_{900}$ (more images are shown in Figure S5, SI section). (d) XRD patterns of the $^{BTn}Fe_{900}$ catalysts treated at 900 °C. (e) EDS mapping of images of $^{BT1}Fe_{900}$ (images of the other materials are shown in Figures S6-S8, SI section).

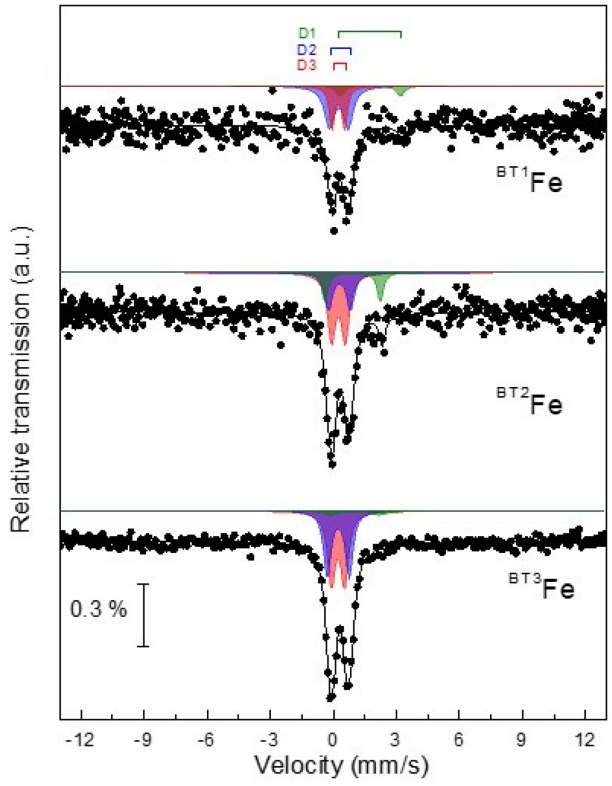

Figure 4. ^{57}Fe Mössbauer spectra measured at room temperature of the samples ^{BTn}Fe. Doublets D2 (blue) and D3 (red) are related to the Fe^{III} ion while the D1 (green) to the Fe^{II} ion (see text).

to the presence of ferrolaueite ($Fe^{II}Fe^{III}_2(PO_4)_2(OH)_2{\cdot}8H_2O$)[33] or phosphoferrite ($(Fe^{II},Mn^{II})_3(PO_4)_2{\cdot}3H_2O$),[33] probably in an amorphous form. The presence of nanoparticles containing phosphorous, as indicated by EDS, support this last attribution for these two doublets. The presence of these minerals justifies the appearance of $FePO_4$ and Fe_3PO_7 phosphates after the catalysts are subjected to high temperature thermal treatments (see below). The small doublet with δ ca. 1.35 mm s^{-1}, ΔE_Q ca. 2.48 mm s^{-1} and absorption area of A ca. 14% that appears in all as-prepared catalysts, is attributed to the Fe^{II} ions that was chelated and reduced by the polyphenols.[6] The formation of Fe^{II} from Fe^{III} promoted by the green tea is explained by the Fe^{III}/Fe^{II} reduction potential (E^0 = +0.77 V) compared to polyphenols (E^0 around +0.4 V).[34,35] BT2 presented the highest TPC, followed by BT3 and BT1, what is in line with the Fe^{II} present in the IONPs. Fe^{II}/Fe^{III}-polyphenol nanomaterials prepared from green tea showed a similar Mössbauer spectrum, with two doublets attributed to Fe^{II} and Fe^{III} corresponding to 67 and 33%, respectively.[34]

^{57}Fe Mössbauer spectra of the samples changed considerably after annealed at 900 ºC (Figure 5). The spectra were fitted with two paramagnetic doublets and a magnetic sextet (Table 4). The doublet with δ ca. 0.28 mm s^{-1} and ΔE_Q ca. 0.66 mm s^{-1} corresponds to $FePO_4$.[36] The second doublet with δ ca. 0.33 mm s^{-1} and ΔE_Q ca. 1.14 mm s^{-1} is attributed to Fe_3PO_7.[36,37] The magnetic sextet parameters are attributed to α-Fe_2O_3-hematite.[38] Therefore, the Mössbauer experiments are in complete agreement with the XRD results, disclosing the formation of $FePO_4$, Fe_3PO_7, and α-Fe_2O_3 after annealed at 900 ºC. The predominant phases in $^{BT1}Fe_{900}$, $^{BT2}Fe_{900}$, and $^{BT3}Fe_{900}$ are Fe_3PO_7, hematite, and $FePO_4$, respectively. The highest amount of $FePO_4$ phosphate is found in the $^{BT3}Fe_{900}$ sample. From Table 4 we can see that after the annealing, the $^{BT3}Fe_{900}$ sample presents the smallest linewidth and consequently the highest degree of crystallinity.[39]

FTIR spectra of the as-prepared ^{BTn}Fe samples (Figure 6a) displayed the main characteristic bands of the polyphenols present in black tea.[6-8] The hydroxyl groups of the tea polyphenols (TP) as well as from adsorbed water can be identified in the large band around 3415 cm^{-1}. The C–H stretching can be observed at 2925 and 2851 cm^{-1}. The band at 1696 cm^{-1} is assigned to carboxylic acids, and the following bands at 1628, 1516, and 1453 cm^{-1} are attributed to the aromatic and aliphatic C–H angular bending modes. C–O bonds show absorptions at 1238 and 1086 cm^{-1}. The FTIR spectra of corresponding heated samples (Figure 6b)

Table 3. Room temperature ^{57}Fe Mössbauer hyperfine parameters[a]

Sample	Site	δ / (mm s^{-1})	ΔE_Q / (mm s^{-1})	Γ / (mm s^{-1})	RA / %	Assignment
^{BT1}Fe	D1	1.95	2.88	0.46	11	Fe^{II}
	D2	0.45	0.90	0.56	68	Fe^{III}
	D3	0.43	0.60	0.30	20	Fe^{III}
^{BT2}Fe	D1	1.11	2.64	0.35	15	Fe^{II}
	D2	0.48	1.04	0.45	29	Fe^{III}
	D3	0.43	0.65	0.46	55	Fe^{III}
^{BT3}Fe	D1	1.22	2.30	0.95	13	Fe^{II}
	D2	0.43	1.05	0.42	39	Fe^{III}
	D3	0.41	0.63	0.44	48	Fe^{III}

[a]Isomer shift (δ), quadrupole splitting (ΔE_Q), linewidth (Γ) and absorption area (A) for the ^{BTn}Fe samples (Figure 4).

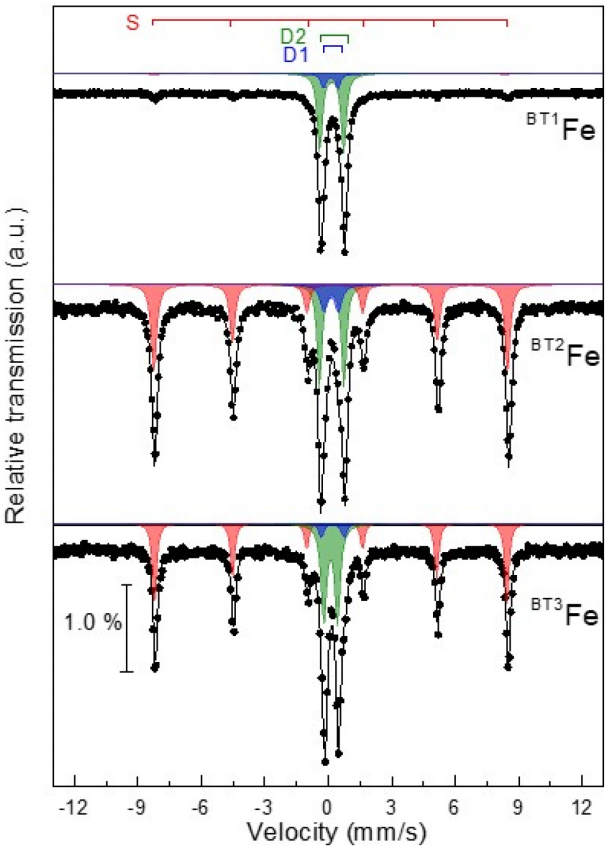

Figure 5. ^{57}Fe Mössbauer spectra measured at room temperature of the $^{BTn}Fe_{900}$ samples. D1 and D2 indicate doublets and S a sextet. The Mössbauer hyperfine parameters of each subspectra are shown in Table 4.

lack the bands of polyphenols and show the characteristic bands of the phases detected by XRD and Mössbauer. The bands between 1700 and 400 cm^{-1} correspond to Fe_3PO_7 and $FePO_4$. The absorptions centered at 1630 and 1462 cm^{-1} may be assigned to P=O, and the bands at 1061 and 1029 cm^{-1} are due the P–O stretching. The bands at 631, 595, 563, and 435 cm^{-1} are assigned respectively to P–O–P, Fe–O stretching and bending deformations (Scheme S1, SI section).[40]

Degradation of methyl orange by Fenton system

The as-prepared ^{BTn}Fe and the annealed samples $^{BTn}Fe_{900}$ were applied as catalyst in the heterogeneous Fenton degradation of the dye methyl orange. The tests followed the experimental conditions previously optimized for similar green iron nanomaterials,[7] 10.0 mg of catalysts (0.5 g L^{-1}), 4.7×10^{-5} mol L^{-1} of MO and 0.69 mol L^{-1} of H_2O_2 at a final volume of 20.0 mL were used, leading to a MO:H_2O_2 molar ratio of 1:14500.

Figure 7a shows the UV-Vis electronic spectra of methyl orange degradation catalyzed by ^{BT2}Fe. The decrease of the band at λ_{max} = 464 nm indicates the break of the azo N=N bond. A red-shift of the azo band was observed from 464 to 474 nm after 30 min, and to 490 nm at the end of the reaction. The MO molecule is a pH indicator, so the displacement of the wavelength indicates pH change during the reaction. Accordingly, the reaction pH was monitored, and it lowered from 6.9 before reaction, to 5.9 after catalyst addition, and respectively to 4.4 after H_2O_2 addition (Table S3, SI section). Finally, after 20 min the pH was 3.4 and continued until the end of the reaction. To confirm that, UV-Vis spectra of aqueous MO solution were taken in different pHs (Figure S12, SI section) and the band wavelength matched with the values observed during the Fenton reaction. These changes are caused by protonation/deprotonation of MO (Scheme S2, SI section), whose speciation depends on the $K_a = 4.0 \times 10^{-4}$. Below pH 1.0 all molecules of MO are protonated and above pH 5.7 they are completely deprotonated (Table S4, SI section).

According to previous publications,[1,2,6-8,13,14] the polyphenols can release protons during the Fenton degradation, and adjusts the reaction pH around 3, which is the ideal pH for Fenton catalysis. This was corroborated by the increase of TOC during the reaction caused by the partial release of the polyphenols from ^{BT2}Fe (Table S5, SI section), adjusting the pH to 3.4.

Table 4. Room temperature ^{57}Fe Mössbauer hyperfine parameters[a]

Sample	Site	δ / (mm s^{-1})	ΔE_Q / (mm s^{-1})	B_{hf} / (mm s^{-1})	Γ / (mm s^{-1})	RA / %	Assignment
$^{BT1}Fe_{900}$	D1	0.28	0.69		0.27	13	$FePO_4$
	D2	0.33	1.16		0.28	74	Fe_3PO_7
	S	0.37	–0.26	51.5	0.72	13	hematite
$^{BT2}Fe_{900}$	D1	0.29	0.68		0.40	15	$FePO_4$
	D2	0.32	1.16		0.28	28	Fe_3PO_7
	S	0.37	–0.19	51.9	0.31	57	hematite
$^{BT3}Fe_{900}$	D1	0.28	0.65		0.29	48	$FePO_4$
	D2	0.38	1.08		0.28	6	Fe_3PO_7
	S	0.37	–0.20	51.7	0.24	46	hematite

[a]Isomer shift (δ), quadrupole splitting (ΔE_Q), linewidth (Γ) and absorption area (A) for the ^{BTn}Fe samples (Figure 5).

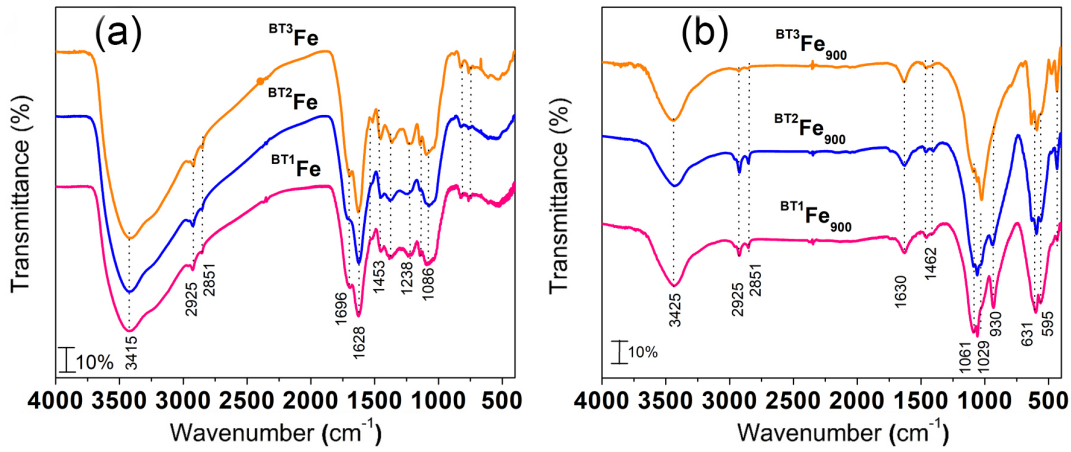

Figure 6. FTIR spectra of the (a) as-prepared ^{BTn}Fe and (b) treated ^{BTn}Fe$_{900}$ samples at 900 °C (normalized curves are shown in Figures S10-S11, SI section).

Figure 7b shows the comparison among all as-prepared catalysts, where more than 90% of degradation was achieved after 5 h.

Control tests were carried out to verify the effectiveness and involvement of the iron nanomaterials in the MO Fenton degradation. A test with the as-prepared and annealed samples and methyl orange without H_2O_2 presented negligible adsorption capacity of the nanomaterials with less than 4% of adsorption. Moreover, the reaction with MO and H_2O_2 without the iron catalysts achieved only 14% of degradation, indicating a low contribution of the homogeneous oxidative process, and the importance of the nanomaterial to catalyze the Fenton process.

Metal leaching of an heterogenous catalyst is always a concerning and in the case of Fenton system, H_2O_2 can accelerate the process. The iron leaching was determined by F AAS, in the supernatant of an aqueous suspension of ^{BT1}Fe or ^{BT1}Fe$_{900}$ in presence of H_2O_2 at the same concentration of the MO degradation tests. ^{BT1}Fe suffered 53% of iron loss during the reaction, representing homogeneous iron concentration of 20.25 mg L^{-1}, while for ^{BT1}Fe$_{900}$ no iron leaching was detected above the limit of detection of the instrument. This estimation is based on the amount of residue from the TG that we assigned to Fe_2O_3, and represented 7.0 wt.% of iron for ^{BT1}Fe (Table S2). Iron leaching was also observed for iron oxide nanomaterials prepared with Yerba mate and black tea extracts anchored in amino-functionalized SiO_2, representing the main drawback of these green nanomaterials.[6]

To account for the homogeneous contribution from the iron leaching of the catalyst during the Fenton degradation, a control test using $FeCl_3{\cdot}6H_2O$ was carried out. Iron(III) at 50.0 mg L^{-1} was used and corresponded to twice the concentration of the leached iron. Negligible removal of MO of 10% was achieved, confirming the contribution of heterogeneous catalysis. Furthermore, recent report has demonstrated the improvement of the tea polyphenols in the conventional homogenous Fenton system using Fe^{II} or Fe^{III} ions.[2] The higher lincomycin degradation was attributed to the pH adjustment, but also because the polyphenols can restore Fe^{II} by reduction of Fe^{III} in the reaction medium, which shows the synergy of the system with greater effect than would be expected from the individual contributions of polyphenols, Fe^{III} and H_2O_2.[2]

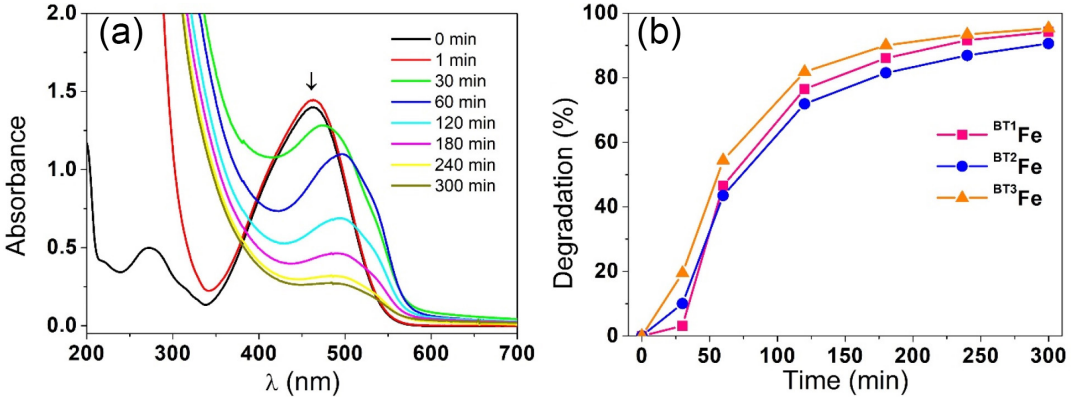

Figure 7. Degradation of methyl orange (4.7 × 10^{-5} mol L^{-1}) at 25 ºC catalyzed by 10.0 mg of catalysts: (a) electronic UV-Vis spectra over time for ^{BT2}Fe, and (b) degradation percentage for all catalysts.

The time trace of the azo band decay for the most efficient catalysts ^{BTn}Fe were fitted with first and second order kinetic models. Figure 8 shows the decrease of the dye over time for ^{BT2}Fe, which the best fit was obtained for pseudo-first order exponential decay shown in equation 2, leading to higher R^2 values. Figure S13 (SI section) shows the linear plots for first and second order that confirmed a better fitting for the first. The UV-Vis spectra and kinetic plots for ^{BT1}Fe and ^{BT3}Fe are presented in Figures S13 and S15 (SI section). The kinetic data and degradation extension are summarized in Table 5. ^{BT3}Fe was the fastest catalyst, with k_{obs} = 0.0122 min^{-1}, and led to the highest degradation, 95%. The observed first-order kinetic constant for the ^{BTn}Fe catalysts are in the range of published Fenton-like system in degradation of lincomycin (LCM) Fe^0/H_2O_2 (k_{obs} = 0.0022 min^{-1}),[1] as well as of green FeONPs prepared from tea polyphenols added to Fe^0 for LCM degradation Fe^0/polyphenol/H_2O_2 (k_{obs} = 0.0556 min^{-1}),[1] and green tea IONPs in degradation of cationic and anionic dyes (k_{obs} = 0.0190 min^{-1}).[11]

$$C_t = C_0 - e^{-k_{obs}t} \quad (2)$$

where C_0 is the concentration of MO at time = 0, C_t is the concentration of MO at given time (t), and k_{obs} is the first-order rate constant.

All annealed catalysts $^{BTn}Fe_{900}$ were considerably less active than the as-prepared materials, reaching less than 30% of degradation (Figure 9). Furthermore, the azo band was not shifted, and the pH dropped slightly from 6.9 to 6.0 and 4.8, after 20 min and at the end of the reaction, respectively, because of the lack of polyphenols in $^{BT2}Fe_{900}$.[41] These results reenforces the importance of the polyphenol proton release to adjust the reaction pH to around 3, and the superior Fenton activity shown by the as-prepared catalysts.

Comparing the annealed materials, $^{BT1}Fe_{900}$ was the most active with 26%, and presented Fe_3PO_7 as the major phase.

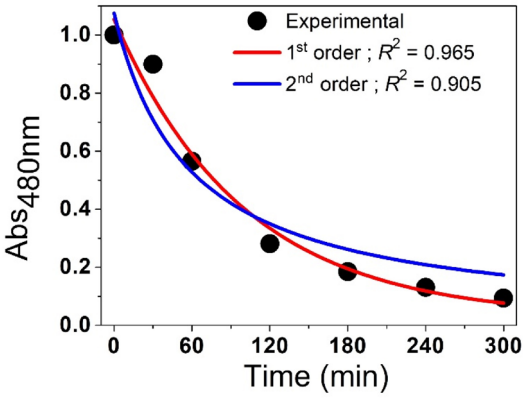

Figure 8. Kinetic experimental data and first- and second-order non-linear fit for MO (4.7×10^{-5} mol L^{-1}) decolorization at 25 °C by a ^{BT2}Fe (10.0 mg).

Table 5. Kinetic data for pseudo-first order equation determined by the non-linear fitting, and degradation of the methyl orange

Catalyst	k_{obs} / min^{-1}	R^2	Decolorization$_{300min}$ / %
^{BT1}Fe	0.0100	0.932	94
^{BT2}Fe	0.0100	0.965	91
^{BT3}Fe	0.0122	0.969	95

k_{obs}: first-order rate constant; R^2: correlation coefficient.

In the other hand, $^{BT2}Fe_{900}$ and $^{BT3}Fe_{900}$ presented α-Fe_2O_3 as the major phase and the lowest activities, 20 and 17%, respectively. Comparing with the IONPs prepared with black tea from Brazil, similar degradation of 34% was achieved. Fenton degradation of methyl orange was carried out using a ultrasmall and conventional α-FeOOH nanorods, achieving a degradation efficiency of 98 and 38% after 60 min, respectively.[42] The material $^{BT2}Fe_{900}$ presented the smallest NPs observed by SEM images, and similar efficiency for the ultrasmall α-FeOOH that shows the positive effect on the MO degradation.[42] Furthermore, $^{BT2}Fe_{900}$ also presented the highest content of α-Fe_2O_3 among the IONPs prepared with black tea, probably indicating the effect of this phase in the catalysis. Kinetic data for the annealed catalysts are shown in Figures S16-S18 (SI section).

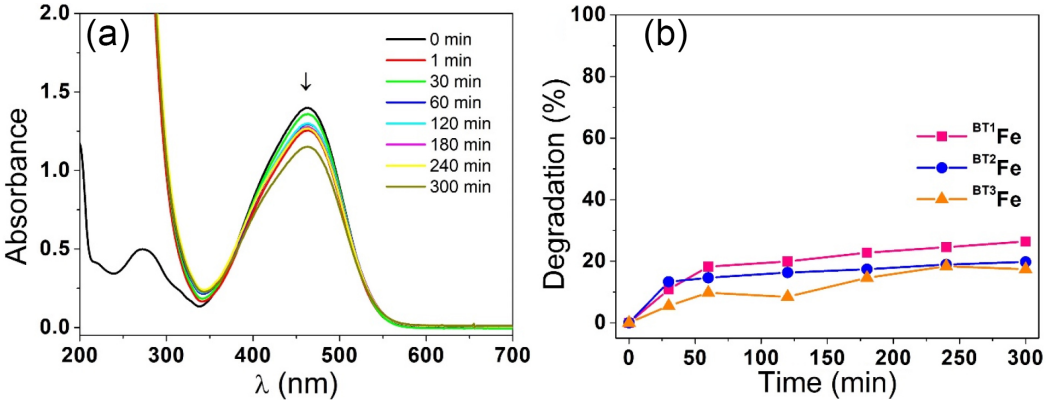

Figure 9. Degradation of methyl orange (4.7×10^{-5} mol L^{-1}) at 25 °C catalyzed by 10.0 mg of catalyst: (a) electronic UV-Vis spectra over time for $^{BT2}Fe_{900}$, and (b) degradation percentage for all catalysts.

Conclusions

Green iron oxides nanomaterials were prepared using *Camellia sinensis* (black tea) extracts of three different regions. Characterization of the as-prepared materials showed the formation of FeOOH, as well as Fe^{III}/Fe^{II} polyphenols complexes indicating chelation and partial reduction of the Fe^{III} precursor to Fe^{II}. Then, the materials were thermally treated at 900 °C and produced α-Fe_2O_3, $FePO_4$ and Fe_3PO_7 phases. The origin of the black led to reproducible materials in terms of phase composition, but with different proportions among the crystalline phases. Furthermore, the phosphorous element come from the plant to form the phosphates. The degradation of the methyl orange dye followed first-order kinetics and was more efficient with the as-prepared materials because of the pH lowering from the polyphenol proton release during the Fenton reaction, adjusting naturally the pH to around 3 that is the optimum pH for Fenton system. In conclusion, this work show that iron crystalline nanomaterials can be formed independent of the black tea origin, using the polyphenols as biotemplates. Although these materials are interesting for the materials point of view, in the Fenton reaction the polyphenols present in the as-prepared materials are important to regulate the pH and led to complete decolorization of methyl orange.

Supplementary Information

Supplementary information (black tea characterization; iron nanoparticles characterization: SEM, EDS, TG, XRD Rietveld refinement, FTIR; methyl degradation data, UV-Vis spectra and kinetic plots) is available free of charge at http://jbcs.sbq.org.br as PDF file.

Acknowledgments

This work was supported by Conselho Nacional de Desenvolvimento Científico e Tecnológico - CNPq (PQ-2/2018), Fundação Carlos Chagas de Amparo à Pesquisa do Estado do Rio de Janeiro - FAPERJ [JCNE: E-26/203.023/2018; Grupos Emergentes: E-26/010.002171/2019); Undergraduated Scholarship: E-26/202.126/2017; Post-doctoral scholarship PDJ10: E-26/290.125/2020] and Coordenação de Aperfeiçoamento de Pessoal de Nível Superior - Brasil (CAPES) (Finance Code 001).We acknowledge DFQ/IQ/UFRJ for the use of S8-Tiger WD FRX spectrometer (FAPERJ), LABNANO/CBPF (Rio de Janeiro) for TEM and SEM measurements in the JEM 2100F Jeol and SEM-FEG 7100FT, respectively. We acknowledge RECAT-UFF for XRD analyses, LCM/CAIPE-UFF for the Raman analyses, and LACES/UFRJ for the thermogravimetric analyses.

Author Contributions

All authors contributed to the formal analysis and writing-review and editing. Raissa T. Franco was responsible for the methodology, investigation, data curation and visualization; Nakédia M. F. Carvalho for conceptualization, methodology, resources, supervision, project administration and funding acquisition; Ana Luisa for validation, resources.

References

1. Ouyang, Q.; Kou, F.; Zhang, N.; Lian, J.; Tu, G.; Fang, Z.; *Chem. Eng. J.* **2019**, *366*, 514. [Crossref]
2. Ouyang, Q.; Kou, F.; Tsang, P. E.; Lian, J.; Xian, J.; Fang, J.; Fang, Z.; *J. Cleaner Prod.* **2019**, *232*, 1492. [Crossref]
3. Teixeira, A. P. C.; Tristão, J. C.; Araujo, M. H.; Oliveira, L. C. A.; Moura, F. C. C.; Ardisson, J. D.; Amorim, C. C.; Lago, R. M.; *J. Braz. Chem. Soc.* **2012**, *23*, 1579. [Crossref]
4. Li, S.; Lo, C.-Y.; Pan, M.-H.; Lai, C.-S.; Ho, C.-T.; *Food Funct.* **2013**, *4*, 10. [Crossref]
5. Del Rio, D.; Stewart, A. J.; Mullen, W.; Burns, J.; Lean, M. E. J.; Brighenti, F.; Crozier, A.; *J. Agric. Food Chem.* **2004**, *52*, 2807. [Crossref]
6. Perrotti, T. C.; Freitas, N. S.; Alzamora, M.; Sánchez, D. R.; Carvalho, N. M. F.; *J. Environ. Chem. Eng.* **2019**, *7*, 103237. [Crossref]
7. Carvalho, S. S. F.; Carvalho, N. M. F.; *J. Environ. Manage.* **2017**, *187*, 82. [Crossref]
8. Trotte, N. S. F.; Aben-Athar, M. T. G.; Carvalho, N. M. F.; *J. Braz. Chem. Soc.* **2016**, *27*, 2093. [Crossref]
9. Majumdar, M.; Khan, S. A.; Nandi, N. B.; Roy, S.; Panja, A. S.; Roy, D. N.; Misra, T. K.; *ChemistrySelect* **2020**, *5*, 13575. [Crossref]
10. Wang, Z.; Fang, C.; Megharaj, M.; *ACS Sustainable Chem. Eng.* **2014**, *2*, 1022. [Crossref]
11. Shahwan, T.; Abu Sirriah, S.; Nairat, M.; Boyaci, E.; Eroĝlu, A. E.; Scott, T. B.; Hallam, K. R.; *Chem. Eng. J.* **2011**, *172*, 258. [Crossref]
12. Heydari, R.; Koudehi, M. F.; Pourmortazavi, S. M.; *ChemistrySelect* **2019**, *4*, 531. [Crossref]
13. Weng, X.; Huang, L.; Chen, Z.; Megharaj, M.; Naidu, R.; *Ind. Crops Prod.* **2013**, *51*, 342. [Crossref]
14. Gao, J.-F.; Li, H.-Y.; Pan, K.-L.; Si, C.-Y.; *RSC Adv.* **2016**, *27*, 22526. [Crossref]
15. De, A.; Kalita, D.; Jain, P.; *ChemistrySelect* **2021**, *6*, 10776. [Crossref]
16. Sriramulu, M.; Balaji; Sumathi, S.; *J. Inorg. Organomet. Polym. Mater.* **2021**, *31*, 1738. [Crossref]

17. Kamaraj, M.; Kidane, T.; Muluken, K. U.; Aravind, J.; *Int. J. Environ. Sci. Technol.* **2019**, *16*, 8305. [Crossref]
18. Khalil, A. T.; Ovais, M.; Ullah, I.; Ali, M.; Shinwari, Z. K.; Maaza, M.; *Green Chem. Lett. Rev.* **2017**, *10*, 186. [Crossref]
19. Franco, R. T.; Silva, A. L.; Licea, Y. E.; Serna, J. D. P.; Alzamora, M.; Sánchez, D. R.; Carvalho, N. M. F.; *Inorg. Chem.* **2021**, *60*, 5734. [Crossref]
20. Raman, C. D.; Kanmani, S.; *J. Environ. Manage.* **2016**, *177*, 341. [Crossref]
21. Zhua, Y.; Zhu, R.; Xi, Y.; Zhu, J.; Zhu, G.; He, H.; *Appl. Catal., B* **2019**, *255*, 117739. [Crossref]
22. Ganiyu, S. O.; Zhou, M.; Martínez-Huitle, C. A.; *Appl. Catal., B* **2018**, *235*, 103. [Crossref]
23. Munoz, M.; de Pedro, Z. M.; Casas, J. A.; Rodriguez, J. J.; *Appl. Catal., B* **2015**, *176-177*, 249. [Crossref]
24. Dias, F. F.; Oliveira, A. A. S.; Arcanjo, A. P.; Moura, F. C. C.; Pacheco, J. G. A.; *Appl. Catal., B* **2016**, *186*, 136. [Crossref]
25. de Souza, A. P. N.; Licea, Y. E.; Colaço, M. V.; Senra, J. D.; Carvalho, N. M. F.; *J. Environ. Chem. Eng.* **2021**, *9*, 105062. [Crossref]
26. Barizão, A. C. L.; Silva, M. F.; Andrade, M.; Brito, F. C.; Gomes, R. G.; Bergamasco, R.; *J. Environ. Chem. Eng.* **2020**, *8*, 103618. [Crossref]
27. Truskewycz, A.; Shukla, R.; Ball, A. S.; *J. Environ. Chem. Eng.* **2016**, *4*, 4409. [Crossref]
28. Vaanamudan, A.; Sarkar, M.; Sadhu, M.; Pamidimukkala, P. S.; *J. Environ. Chem. Eng.* **2019**, *7*, 103244. [Crossref]
29. Salgado, P.; Márquez, K.; Rubilar, O.; Contreras, D.; Vidal, G.; *Appl. Nanosci.* **2019**, *9*, 371. [Crossref]
30. Moore, P. B.; Araki, T.; *Inorg. Chem.* **1976**, *15*, 316. [Crossref]
31. Lawrinenko, M.; Laird, D. A.; van Leeuwen, J. H.; *ACS Sustainable Chem. Eng.* **2017**, *5*, 767. [Crossref]
32. Patterson, A. L.; *Phys. Rev.* **1939**, *56*, 978. [Crossref]
33. Dyar, M. D.; Jawin, E. R.; Breves, E.; Marchand, G.; Nelm, M.; Lane, M. D.; Mertzman, S. A.; Bish, D. L.; Bishop, J. L.; *Am. Mineral.* **2014**, *99*, 914. [Crossref]
34. Markova, Z.; Novak, P.; Kaslik, J.; Plachtova, P.; Brazdova, M.; Jancula, D.; Siskova, K. M.; Machala, L.; Marsalek, B.; Zboril, R.; Varma, R.; *ACS Sustainable Chem. Eng.* **2014**, *2*, 1674. [Crossref]
35. Wang, Z.; *ACS Sustainable Chem. Eng.* **2013**, *1*, 1551. [Crossref]
36. Gadgil, M. M.; Kulshreshtha, S. K.; *J. Solid State Chem.* **1994**, *113*, 15. [Crossref]
37. Sobolev, A. V.; Akulenko, A. A.; Glazkova, I. S.; Pankratov, D. A.; Presniakov, I. A.; *Phys. Rev. B* **2018**, *97*, 104415. [Crossref]
38. Murad, E.; *Hyperfine Interact.* **1998**, *117*, 39. [Crossref]
39. Greenwood, N. N.; Gibb, T. C.; *Mössbauer Spectroscopy*; Chapman and Hall Ltda.: London, 1971.
40. Cipriani, C.; Mellini, M.; Pratesi, G.; Viti, C.; *Eur. J. Mineral.* **1997**, *9*, 1101. [Crossref]
41. Hsueh, C. L.; Huang, Y. H.; Wang, C. C.; Chen, C. Y.; *Chemosphere* **2005**, *58*, 1409. [Crossref]
42. Liu, Z.; Zhang, L.; Dong, F.; Dang, J.; Wang, K.; Wu, D.; Zhang, J.; Fang, J.; *ACS Appl. Nano Mater.* **2018**, *1*, 4170. [Crossref]

Submitted: July 31, 2022
Published online: November 10, 2022